Ultrathin Resistive Sheets for Broadband Coherent Absorption and Symmetrization of Acoustic Waves

M. Farooqui, Yves Aurégan, V. Pagneux

Ultrathin resistive sheets for broadband absorption and symmetrization of acoustic waves

M. Farooqui,* Y. Aurégan,† and V. Pagneux‡
Laboratoire d'Acoustique de l'Université du Mans (LAUM), UMR 6613 CNRS, Le Mans Université, Avenue O. Messiaen, 72085 LE MANS CEDEX 9, France
(Dated: December 8, 2021)

Manipulation of acoustical waves is experimentally and theoretically investigated based on the concept of coherent perfect absorption. It is shown that the absolute control of antisymmetric modes of an acoustic duct is possible using an ultrathin wiremesh. By varying the relative phase of two counter-propagating (normal/oblique) incident waves, absorption from a wiremesh can be tuned from zero to unity. Experimental as well as numerical results demonstrate that this phenomenon is extremely broadband, allowing for instance the symmetrization of the acoustical wave with short pulse in the time domain.

The search for new ways of absorbing waves is still very active and more particularly in acoustics due to the continuous demand in noise control for quiet environment. The most classical sound absorbers are made of porous parts that allow broadband attenuation at high frequencies but that remain low-pass filter and thus inefficient at low frequencies. In the last decade, many types of metamaterial absorbers [1–4] have been proposed. They all are based on the use of subwavelength resonances with finely tuned parameters that provide up to perfect absorption near the resonance frequencies, and are inherently inefficient in the limit of zero frequency. One step further has been achieved recently by the introduction of the Coherent Perfect Absorber (CPA) idea to control and to tune the rate of absorption [5–8]. It corresponds to the time reversal of a laser [5, 6, 9] and it uses the tuning of the incident waves from each side of the absorber.

It appears that a challenging task remains: to absorb sound near the zero frequency limit while remaining broadband. Indeed, when using typical subwavelength resonators the quality factor of the peak of absorption the resonance frequency increases when this frequency goes to zero [10, 11]. To avoid resonance is a solution to obtain broadband low frequency absorption as demonstrated by metallic conductive films [12, 13], where CPA with total absorption is possible. In the domain of airborne acoustics, ultrathin millimetric resistive sheets offer the same possibilities [14, 15]. Often called wiremesh, their efficiency has no lower bound limit on frequency; they are used even for static flow, for instance in filtration, and they remain efficient up to high frequencies as long as the wavelength is larger than the millimetric thickness.

In this letter, we present experimental and numerical evidences of the low and mid frequency absorption possibilities of the ultrathin resistive sheets. After showing the capabilities of CPA for scattering, we apply it in a symmetric closed cavity where it has important and natural impacts: when the absorber is at the center of symmetry of the cavity the antisymmetric waves are totally absorbed. Since the resistive sheets are very thin compared to audible airborne acoustic typical wavelengths the cancellation of antisymmetric acoustic field is very broadband and it allows us to demonstrate it experimentally in the time domain with short pulses. We also take advantage of the wide bandwidth of this effect to design cavities where the sound field is symmetrized independently of the source position on a broad frequency range.

Let us begin by a description of the system at hands. In acoustics, a resistive screen can be made of a thin porous material and the simplest realization is a very fine mesh cloth referenced in the following as wiremesh. Through such a screen, the acoustic velocity is continuous and the pressure p, described elsewhere by the Helmholtz equation: $\nabla^2 p + k^2 p = 0$, makes a jump at the screen which is given by:

$$[\partial_n p]_s = 0 \quad \text{and} \quad [p]_s = -(Z/\mathrm{i}k)\,\partial_n p \tag{1}$$

where ∂_n denotes the normal derivative, $k = \omega/c_0$ is the wavenumber, ω is the frequency, c_0 is the speed of sound and Z is the screen impedance normalized by $\rho_0 c_0$. With the $\exp(-\mathrm{i}\omega t)$ convention that is chosen here, there is absorption if $\Re(Z) > 0$. As long as viscous effects dominate inertial effects, this screen is purely resistive, $|\Im(Z)| \ll \Re(Z)$, and the resistance is proportional to the viscosity and depends on the wire diameter, the type of weave and the size of the apertures. Consequently, the purely resistive wiremesh considered in the following is modelled by a positive real Z independent of the frequency.

Due to its high flexibility and to avoid vibration, it is advantageous to bond the wiremesh to a more rigid perforated plate, see Fig. 1a (in the following we will simply call wiremesh the assembly of these two thin parts). The resistance of the assembly is then given by the product of the intrinsic resistance of the wiremesh by the percentage of open area (POA) of the perforated plate.

In the particular case of a plane wave at normal incidence to the screen, the problem becomes unidimensional and the reflection and transmission coefficients are writ-

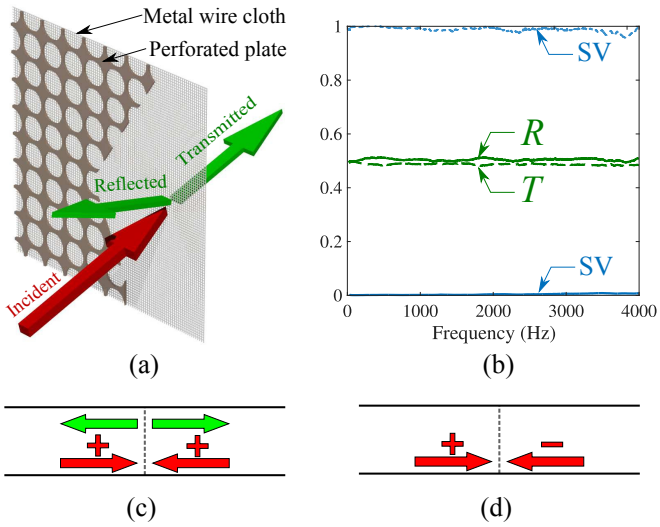

FIG. 1. Generic wiremesh absorber (a) Schematic of the absorber illuminated by unidirectional acoustic wave, (b) Measured absolute values of the reflection $|R|$ and transmission $|T|$ coefficients. The SVDs are the measured singular values of the scattering matrix. (c) Symmetrical and (d) antisymmetrical cases displaying respectively zero and perfect absorption.

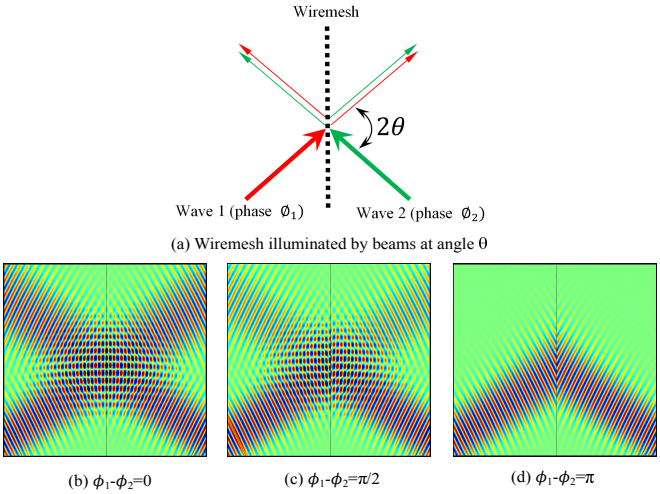

FIG. 2. Numerical simulation of an incident Gaussian beam on wiremesh $Z = 2/\cos(\theta)$, (a) Schematic drawing of the wiremesh with incident Gaussian beams at oblique angle $\theta = \pi/6$, (b) Symmetrical case ($\phi_1 - \phi_2 = 0$), (c) Intermediate case ($\phi_1 - \phi_2 = \pi/2$), and (d) Antisymmetrical case ($\phi_1 - \phi_2 = \pi$)

ten as:

$$R = Z/(2+Z) \quad \text{and} \quad T = 2/(2+Z), \tag{2}$$

and the absorption coefficient for an incident wave on one side is:

$$\alpha = 1 - |R|^2 - |T|^2 = \frac{1}{2}\left(1 - \left|\frac{Z-2}{Z+2}\right|^2\right) \tag{3}$$

The resistance $Z = 2$ maximizes the absorption coefficient of the screen $\alpha = 1/2$ when the incident wave is only on one side of the screen [16, 17]. In this case, the reflection and transmission coefficients are also equal to

$$R = T = 1/2. \tag{4}$$

Fig. 1b displays the measured reflection (R) and transmission (T) coefficients of an assembly of a wiremesh of resistance 1.02 with a perforated plate with a POA of 50% leading to an impedance very close to $Z = 2$. These measured coefficients are nearly equal to 1/2 in a hyper-wide frequency band extending from zero frequency to the maximum measurement frequency given by the cut-off frequency of the measuring tube.

The two singular values (SV) of the scattering matrix,

$$S = \begin{pmatrix} R & T \\ T & R \end{pmatrix}, \tag{5}$$

correspond to the maximum and minimum outgoing wave fluxes for any incoming waves with unit flux. They are given by:

$$\sigma_S = 1 \quad \text{and} \quad \sigma_A = \left|\frac{Z-2}{Z+2}\right| \tag{6}$$

which correspond respectively to the symmetrical (Fig. 1c) and antisymmetrical (Fig. 1d) cases [18]. When $Z = 2$, these SVs are theoretically as well as experimentally equal to 1 and 0 (see Fig. 1b). In the symmetrical case, there is no dissipation and everything works as if the screen were not present. In the antisymmetrical case, the waves are completely absorbed and the screen becomes a CPA [5, 19]. In particular, it can be noted that the measured singular value σ_A which corresponds to the CPA never exceeds 0.008 for all measured frequencies.

This CPA effect is further illustrated in Fig. 2 where two Gaussian beams of same amplitude are incident on the screen with the same angle θ and at the same point. In this case, $\sigma_S = 1$ and $\sigma_A = |(\cos(\theta)Z - 2)/(\cos(\theta)Z + 2)|$. Thus the optimal impedance varies according to the inclination of the wave with $Z = 2/\cos(\theta)$. It can be seen that when the two waves are in phase (Fig. 2b) the waves propagate, far from the screen, as if the screen were not there. On the contrary, when the two incident waves are of opposite phase (Fig. 2d) they are completely absorbed (CPA). For an intermediate phase, the waves are partially absorbed, Fig. 2c.

In view of the previous results, it appears that using a wiremesh resistive screen in acoustics leads to CPA with a huge subwavelength ratio. In our experiment, the total thickness of the wiremesh is 1.2 mm while the lowest measured frequency is 50 Hz (see Fig. 1): it leads to a subwavelength ratio of 6800 as well as a hyper-wide frequency band. We insist that the prefix "hyper" refers here to the fact that the CPA operates from zero frequency limit (here measured down to 50 Hz due to loudspeaker limitations) to the cut-off frequency of the duct

(here around 6 kHz). An interesting aspect is that such a large bandwidth opens the possibility to extend the CPA effect into the time domain. For a scattering problem it would be obvious that short wavepackets incident from both sides and with good phase adjustment would lead to total absorption (by a simple Fourier transform argument of the previous results). We choose now to go one step further by using the symmetry of closed cavities to provide the phase coherence ingredient in CPA. Indeed, it appears that a mirror symmetric cavity naturally allows to decompose the wave into components with different parities (i.e. symmetric and antisymmetric). Thus, parity and phase coherence coming together, the CPA effect is accomplished by locating the wiremesh at the symmetry axis. To explore this aspect in an actual experiment, we consider a closed duct of length $2L$ ($L = 405$ mm) in which the CPA wiremesh (with $Z = 2$) is placed at the mid-position (the symmetry axis). At the left extremity of the duct we sent a pulse through a small orifice [20] and two microphones M_1 and M_2 are located at the two extremities, see Fig. 3a. The incident pulse signal is measured at M_1 by windowing the multiple echoes (Fig. 3b). First, as a reference, when the wiremesh is not present, the pressure signals are displayed in Fig. 3c, where the incident pulse is reproduced every 4 τ (where $\tau = L/c_0$ =1.18 ms is half the time of flight between the two microphones) since the wave is reflected at both extremities of the duct [21]. Then, in the presence of the wiremesh, the situation is clearly different with equal signals at both ends from early time 2 τ (Fig. 3d). The reason for this symmetrization of the pressure in the duct is simple: when the pulse reaches the screen (at time τ), it is half transmitted and half reflected, and, from that instant, the sound field becomes completely symmetrical with respect to the middle of the duct, reaching the symmetrical microphones at 2 τ. It can be noticed that the equal amplitude of the two pulses on each side of the screen corresponds to half the amplitude of the incident wave.

The symmetrization of the acoustic field by introducing a CPA wiremesh at the symmetry axis of a cavity can also be observed in the frequency response spectrum. In the same experimental setup as described above, in order to detect the resonance frequencies of the closed duct, we now measure the transfer function defined as the ratio of the pressure at microphone M2 with the voltage applied to the source (approximately proportional to the flow rate of the source), see Fig. 4. Without wiremesh (red line), the peaks correspond to the modes of a closed tube of length $2L$ and are given by $f_n = n\, c_0/4L$ where $c_0/4L$ = 211.5 Hz and n= 1, 2, ... When the wiremesh is inserted at the mid-position of the tube (dashed blue line), half of the modal resonances are suppressed. The cut-off resonances correspond to antisymmetric modes while the resonances associated with symmetric modes remain unchanged. This effect of suppression of the antisymmetric modes and thus of symmetrization of the resonances is described in the Supplemental Material by a simple one-dimensional model.

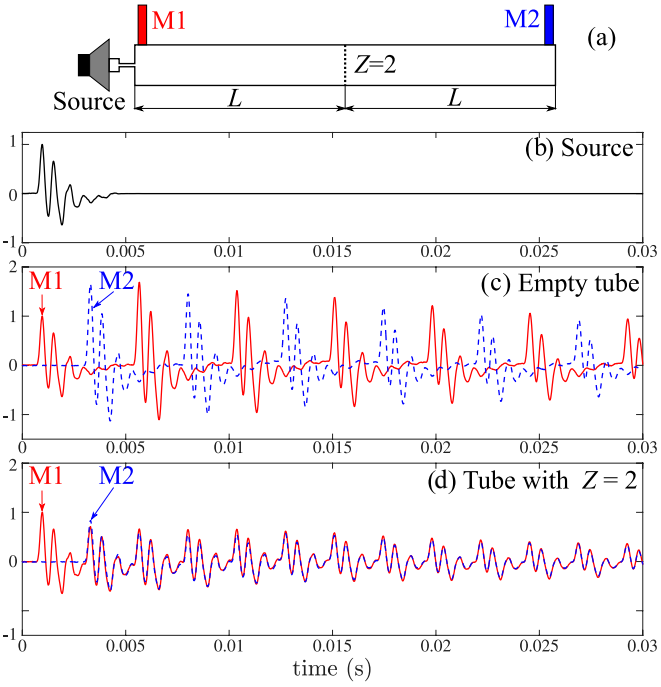

FIG. 3. Measured temporal signals (a) sketch of the experimental setup (b) Input signal from the source (c) Measured responses at microphones M1 (solid red) and M2 (dashed blue) for an empty tube, (d) Measured responses at M1 and M2 for tube with $Z = 2$ wiremesh

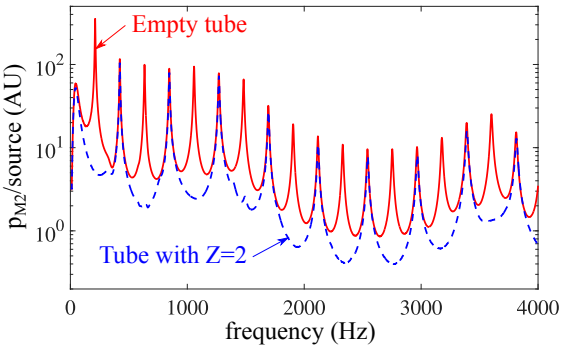

FIG. 4. Experimental results for the transfer function $p_{M2}/source$ in the same geometry as in Fig. 3(a) for an empty tube (solid red) and for a tube with $Z = 2$ wiremesh (dashed blue)

Rather surprisingly, this antisymmetric mode suppression by a resistive screen is robust to geometric changes and is maintained even when the symmetric geometry has a variable cross-section. To illustrate this phenomenon, two different symmetric geometries are considered in Fig. 5. The first is a bi-triangular duct, Fig. 5a, while the second is a duct loaded by side cavities,Fig. 5b. For a given

source at point S, the frequency response spectrum at point P is numerically computed using COMSOL Multiphysics and results are displayed in Fig. 5c-d with and without a resistive screen of impedance $Z = 2$ located in the symmetry plane. It appears that the resonances associated to antisymmetric modes are suppressed for both geometries as in the constant section case. Thus the antisymmetric suppression occurs even when the waves are not plane and normal to wiremesh. We can see such behavior in Fig. 5a, for the mode at $kH = 2.1$ which exhibits that wiremesh is effective even on higher order modes. However, the suppression effect is diminished possibly for modes with high angle of inclination on the wiremesh as in Fig. 5d at $kH = 1.5$.

This work demonstrates experimentally and theoretically the control of antisymmetric acoustic waves in ducts using a ultrathin resistive screen. It is based on the concept of coherent perfect absorption, and since the ultrathin sheets are of purely resistive nature, their effects are not linked to a resonance phenomenon. Consequently, the symmetrization of the acoustic waves is extremely broadband, starting from zero frequency, and can even be exhibited in the time domain with short pulses. In addition, it is shown that this symmetrization effect is robust to variations of the duct cross-section. This work opens up the possibility of creating ultrathin noise controllers and attenuators that are simultaneously extremely broadband and ultra-subwavelength.

This work was supported by the International ANR project FlowMatAc a cooperation project between France and Hong Kong (ANR-15-CE22-0016-01). The authors thank Svetlana Kuznetsova, Christian Morfonios and Malte Rontgen for careful readings of the manuscript.

* maaz.farooqui@univ-lemans.fr
† yves.auregan@univ-lemans.fr
‡ vincent.pagneux@univ-lemans.fr

[1] N. I. Landy, S. Sajuyigbe, J. J. Mock, D. R. Smith, and W. J. Padilla, Physical review letters **100**, 207402 (2008).
[2] C. M. Watts, X. Liu, and W. J. Padilla, Advanced materials **24**, OP98 (2012).
[3] J. Mei, G. Ma, M. Yang, Z. Yang, W. Wen, and P. Sheng, Nature communications **3**, 1 (2012).
[4] M. Yang and P. Sheng, Annual Review of Materials Research **47**, 83 (2017).
[5] Y. Chong, L. Ge, H. Cao, and A. D. Stone, Physical review letters **105**, 053901 (2010).
[6] W. Wan, Y. Chong, L. Ge, H. Noh, A. D. Stone, and H. Cao, Science **331**, 889 (2011).
[7] D. G. Baranov, A. Krasnok, T. Shegai, A. Alù, and Y. Chong, Nature Reviews Materials **2**, 1 (2017).
[8] A. Müllers, B. Santra, C. Baals, J. Jiang, J. Benary, R. Labouvie, D. A. Zezyulin, V. V. Konotop, and H. Ott, Science advances **4**, eaat6539 (2018).
[9] S. Longhi, Physics **3**, 61 (2010).
[10] M. Yang, S. Chen, C. Fu, and P. Sheng, Materials Horizons **4**, 673 (2017).
[11] Y. Aurégan, Applied Physics Letters **113**, 201904 (2018).
[12] G. Nimtz and U. Panten, Annalen der Physik **19**, 53 (2010).
[13] S. Li, J. Luo, S. Anwar, S. Li, W. Lu, Z. H. Hang, Y. Lai, B. Hou, M. Shen, and C. Wang, Physical Review B **91**, 220301 (2015).
[14] U. Ingard, *Noise reduction analysis* (Jones & Bartlett Publishers, 2009).
[15] A. Coutant, Y. Aurégan, and V. Pagneux, The Journal of the Acoustical Society of America **147**, 3124 (2020).
[16] E. Plum, K. F. MacDonald, X. Fang, D. Faccio, and N. I. Zheludev, ACS Photonics **4**, 3000 (2017).
[17] C. Meng, X. Zhang, S. T. Tang, M. Yang, and Z. Yang, Scientific reports **7**, 43574 (2017).
[18] A. Merkel, G. Theocharis, O. Richoux, V. Romero-García, and V. Pagneux, Applied Physics Letters **107**, 244102 (2015).
[19] V. Romero-García, G. Theocharis, O. Richoux, A. Merkel, V. Tournat, and V. Pagneux, Scientific reports **6**, 19519 (2016).
[20] The small size of the orifice, whose diameter is 1 mm, compared to the diameter of the duct (30 mm) makes it possible to consider that it has little influence on the acoustic response of the duct cavity.
[21] It can be noted that since the microphones are very close to the walls, they measure at the same time both the incident wave and the reflected pulses and the signal is doubled compared to the incident pulse.

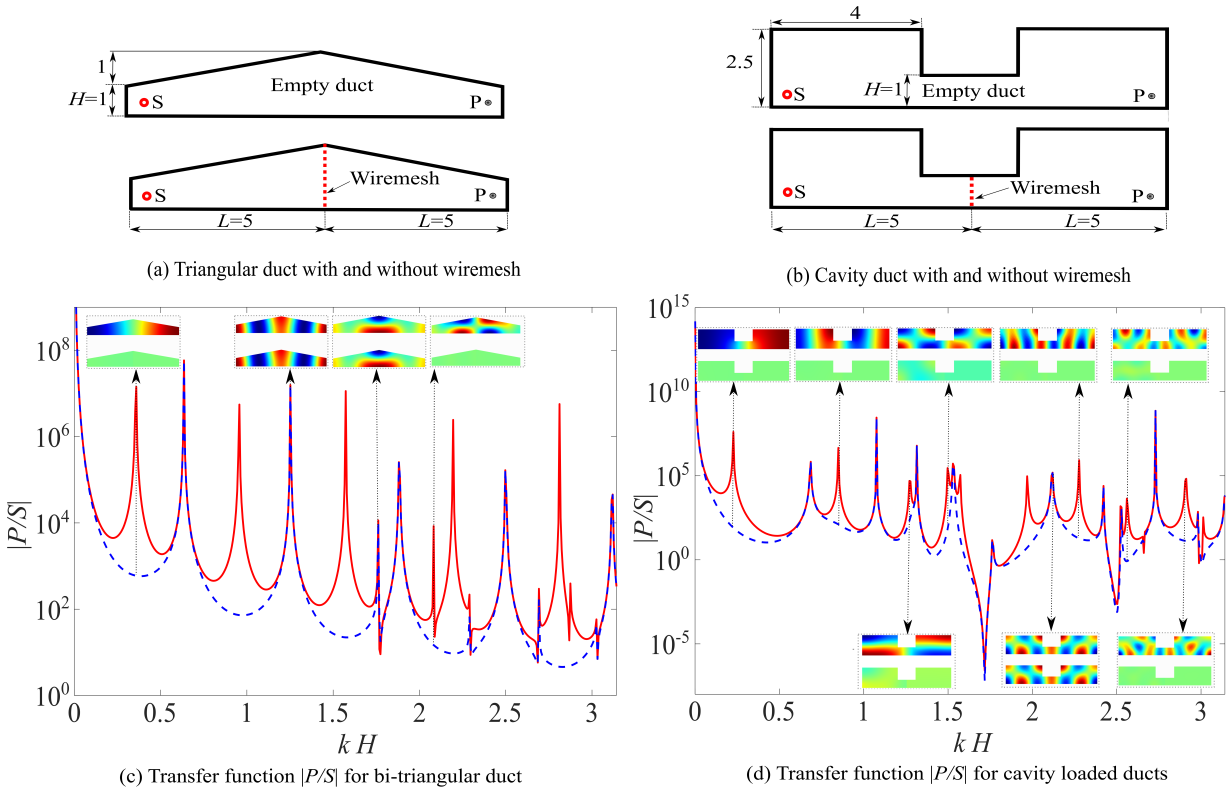

(a) Triangular duct with and without wiremesh

(b) Cavity duct with and without wiremesh

(c) Transfer function $|P/S|$ for bi-triangular duct

(d) Transfer function $|P/S|$ for cavity loaded ducts

FIG. 5. Transfer function $|P/S|$ calculations for ducts of variable cross-section with and without $Z = 2$ wiremesh where S is a monopole source strength at point S and P is the pressure at point P. (a) Empty bi-triangular geometry (top) and with $Z = 2$ wiremesh (bottom), (b) Empty cavity loaded geometry (top) and with $Z = 2$ wiremesh (bottom), (c) Variation of $|P/S|$ with respect to k for bi-triangular ducts and (d) Variation of $|P/S|$ with respect to kH for cavity loaded ducts

Supplemental material: One dimensional model of the cavity with a resistive sheet

I. CALCULATION OF THE MODES

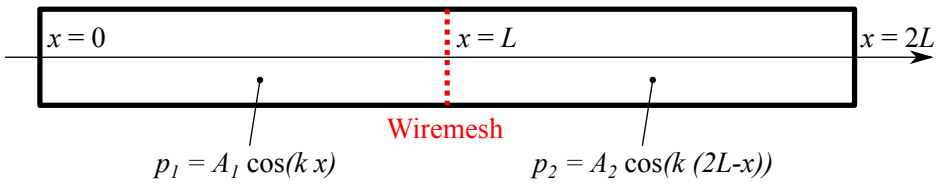

FIG. 1. One dimensional analysis of acoustic field in a duct with thin wiremesh

To compute the modes in a duct of length $2L$ with thin wiremesh at the center (see Fig. 1), the acoustic field can be written as $p_1 = A_1 \cos(kx)$ for $0 < x < L$ and $p_2 = A_2 \cos(k(2L - x))$ for $L < x < 2L$. At the wiremesh position, the continuity of velocity and the impedance relation that have been wrtitten as

$$[p']_L = 0 \quad \text{and} \quad [p]_L = (-Z/\mathrm{i}k)\, p' \tag{1}$$

lead to

$$(A_1 + A_2)\sin(kL) = 0 \tag{2}$$

$$(A_1 - A_2)\cos(kL) = \mathrm{i}ZA_1 \sin(kL). \tag{3}$$

which eventually conduct to the dispersion relation

$$\mathcal{D} = \sin(kL)(2\cos(kL) - \mathrm{i}Z\sin(kL)) = 0. \tag{4}$$

When $Z = 0$, two sets of solutions exist: one with $\sin(kL) = 0$ ($A_1 = A_2$) and the other with $\cos(kL) = 0$ ($A_1 = -A_2$). They correspond respectively to the symmetric and antisymmetric modes of the empty tube of length $2L$.

When Z is different from 0, the symmetric modes ($\sin(kL) = 0$ and $A_1 = A_2$) keep real eigenfrequencies k; actually they do not feel the presence of the wiremesh because they $p' = 0$ at $x = L$ (see equation (1)). On the other hand, the eigenfrequencies of the antisymmetric modes are no longer real as can be seen in Fig. 2. These modes progressively acquire a negative imaginary part while their real parts remain equal to $n\pi/2$ ($n = 1, 2, 3, ...$). For $Z = 2$, these modes disappear

with an imaginary part that tends to infinity. For a resistance higher than 2, they reappear from infinity and return to the symmetrical modes with a real part equal to $m\pi$ ($m = 0, 1, 2, ...$). Why $Z = 2$ is so special for the antisymmetric modes? This can be seen if we use the symmetry of the system that allows us to decompose the eigenproblem into 2 subproblems; one for the symmetric modes and one for the antisymmetric modes. For the antisymmetric problem, we arrive at the wave equation with boundary conditions : $p = 0$ at $x = 0$ and $ikp = (Z/2)p$ at $x = L$. It is then clear that for $Z = 2$, these boundary conditions ($p = 0$, ie hard wall, and $p = ikp$, ie wave totally radiating to the right) correspond the problem of a semi-infinite tube that is known to have no resonance frequencies at all.

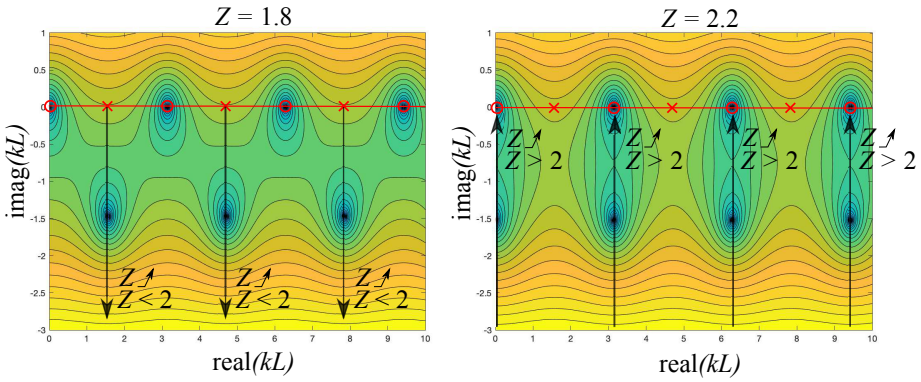

FIG. 2. Colour map of $|\mathcal{D}|$ for two values of the resistance Z. Blue values correspond to $|\mathcal{D}| = 0$. Symmetric modes marked with red circles do not move. The antisymmetric modes (indicated by a red $\times$ at $Z = 0$) acquire a negative imaginary part when Z moves away from 0. The imaginary part becomes larger and larger until the modes disappear at infinity for $Z = 2$. For a resistance higher than 2, these modes return from infinity to the symmetrical modes (red circles).

II. CALCULATIONS WITH A SOURCE

When a point source is placed inside a rigid duct at $x = x_0$ (see Fig. 3), the Helmholtz equation with point source can be written in the form

$$p'' + k^2 p = \delta(x - x_0). \tag{5}$$

The presence of the source at $x = x_0$ gives two relations linking the pressure and its derivative on both sides of the source at $x = x_0$: $[p']_{x_0} = 1$ and $[p]_{x_0} = 0$. To simplify the solution of this problem, it can be considered as the sum of two problems, one symmetric and the other antisymmetric: $p(x) = p_s(x) + p_a(x)$ (see Fig. 3).

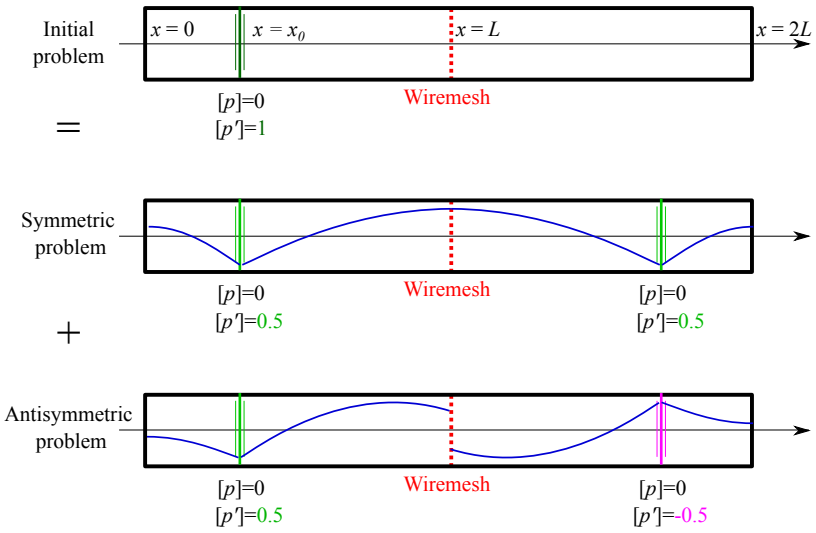

FIG. 3. One-dimensional problem in a duct in the presence of a wiremesh and with a source considered as the addition of a symmetric problem and an antisymmetric problem.

For the symmetric problem, the pressure derivative always vanishes on the wiremesh ($x = L$) which can therefore be considered as a rigid wall ($p_s'(L) = 0$). The symmetric solution can then be written:

$$p_s = S_1 \cos(kx) \quad 0 < x < x_0, \tag{6}$$

$$p_s = S_2 \cos(k(x - L)) \quad x_0 < x < L, \tag{7}$$

where S_1 and S_2 are given by

$$2k \sin(kL) S_1 = -\cos(k(L - x_0)), \tag{8}$$

$$2k \sin(kL) S_2 = -\cos(kx_0). \tag{9}$$

For the antisymmetric problem, the pressure and its derivative for $x < L$ are linked at the wiremesh by

$$p_a(L) = \frac{Z}{2\mathrm{i}k} p_a'(L) \tag{10}$$

Then, the antisymmetric pressure can be written

$$p_a = A_1 \cos(kx) \quad 0 < x < x_0, \tag{11}$$

$$p_a = A_2(\sin(k(L - x)) + \mathrm{i}Z/2 \ \cos(k(L - x)) \quad x_0 < x < L, \tag{12}$$

where A_1 and A_2 are given by

$$k[2\cos(kL) - \mathrm{i}Z \sin(kL)]A_1 = \mathrm{i}Z/2 \ \cos(k(L - x_0)) + \sin(k(L - x_0)), \tag{13}$$

$$k[2\cos(kL) - \mathrm{i}Z \sin(kL)]A_2 = \cos(kx_0). \tag{14}$$

A plot of these solutions is given in Fig. 4.

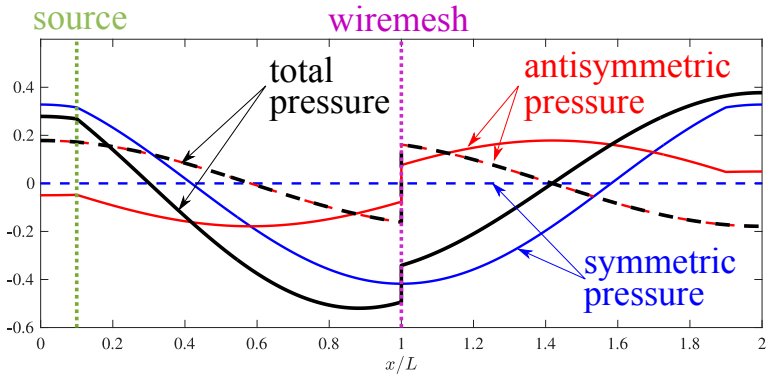

FIG. 4. Pressure in the tubes for $Z = 2$, $kL = 2.7$ and $x_0 = 0.1L$. The solid lines are the real part of the pressure while the dashed lines are the imaginary part. In blue the symmetric pressure p_s, in red the antisymmetric pressure p_a and in black the total pressure $p = p_s + p_a$.

In order to compare these one-dimensional results with the experimental results, the source is placed on one of the walls by setting $x_0 = 0$. The pressure is calculated at the point where there is a microphone, i.e. at $x = 2L$. The total pressure at the microphone is then equal to $p_t(2L) = p_s(0) - p_a(0)$. The symmetric and antisymmetric pressure are

$$p_s(0) = -\frac{\cos(kL)}{2k\sin(kL)}, \quad p_a(0) = \frac{2\sin(kL) + \mathrm{i}Z\cos(kL)}{2k(2\cos(kL) - \mathrm{i}Z\sin(kL))} \tag{15}$$

As it can be seen in Fig. 5, the calculations compare qualitatively well with the experimental results: the presence of a wiremesh of resistance $Z = 2$ makes the antisymmetric modes disappear. A more quantitative comparison is not possible here because the acoustic flow rate of the source was not measured during the experiments. The one-dimensional calculations can therefore be used to predict the effect of a resistive sheet in a tube quite easily (see Fig. 6).

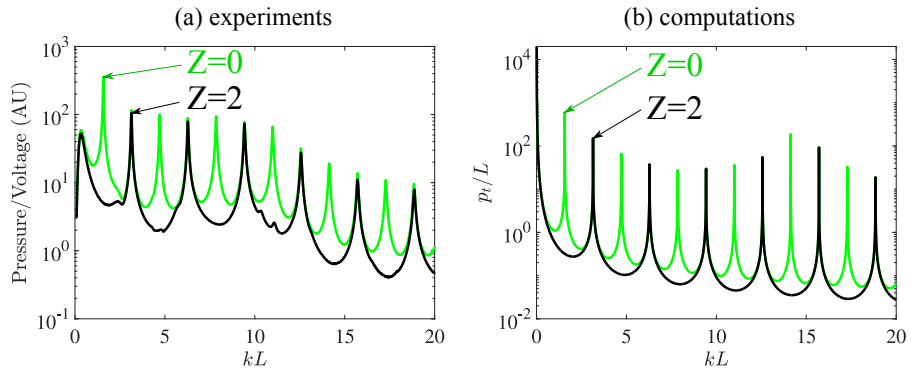

FIG. 5. Comparison of the ratio between the pressure at $x = 2L$ and the source at $x = 0$ (a) experimental results (b) one-dimensional calculations. The green curves correspond to an empty tube ($Z = 0$) and the black curves to a tube with a wiremesh $Z = 2$. We see that half of the resonance peaks (corresponding to antisymmetric modes) are suppressed for Z=2.

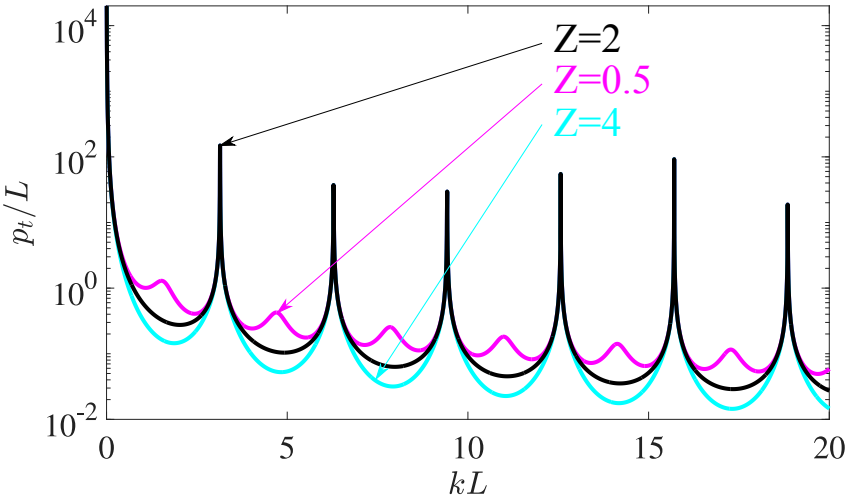

FIG. 6. Ratio between the pressure at $x = 2L$ and the source at $x = 0$ for 3 different values of the resistance. Black: $Z = 2$, magenta: $Z = 0.5$, cyan: $Z = 4$.